J Appl Electrochem (2009) 39:1739–1744
DOI 10.1007/s10800-009-9868-4

ORIGINAL PAPER

Anodic behavior of indium in KOH solution

Hebing Zhou · Mengqing Xu · Qiming Huang · Zongping Cai · Weishan Li

Received: 1 August 2008 / Accepted: 6 March 2009 / Published online: 21 March 2009

Abstract Cyclic voltammetry (CV) and X-ray diffraction (XRD) were used to investigate the anodic behavior of indium in a 3 M KOH solution on both rotating disc-platinum ring and static electrodes. Indium undergoes two processes in concentrated alkaline solution: activation and passivation. In the activation region, soluble, tri-valent indium is the main product, generated by the disproportionation reaction of $In(OH)_{ad}$ in the initial stage, and direct oxidation of indium during the latter stage. The soluble, trivalent indium accumulates and precipitates as $In(OH)_3$ on the electrode surface, inhibiting the oxidation of indium. In the resulting passivation region, the indium under the precipitated $In(OH)_3$ is oxidized to In_2O_3, which is more stable than $In(OH)_3$, and prevents further oxidation of the indium.

Keywords Indium · Alkaline solution · Anodic behavior · Rotating ring-disc electrode · Mechanism

1 Introduction

Indium is a valuable metal, with high corrosion resistance and a high hydrogen evolution overvoltage [1]. Indium and its oxide have been widely used in the electronic and optoelectronic industries. Examples are as a transparent electrode for display systems, solar energy heat mirrors, and window layers in heterojunction solar cells [2–14]. More applications are being found in various industrial areas. Recently, indium and its oxide have been successfully used as a substitute for mercury in alkaline zinc batteries [15–17]. Depositing a thin layer of indium on the surface of the negative zinc plate and current collector suppresses self-discharge of the batteries. The electrochemical behavior of indium in acidic and weak alkaline solutions has been widely reported [18–24], but is less well understood in an alkaline solution [25–28] such as the electrolyte for a zinc-air high-energy battery.

Saidman et al. reported the electrochemical behavior of indium in NaOH solutions of various concentrations [25], and suggested that the anodic reaction of indium was a function of the NaOH concentration. It appeared that the anodic process at $\leq$1 M (mol L^{-1}) hydroxyl ion (OH^-) concentrations involved only one oxidation step, forming a stable compact film of $In(OH)_3$. In much more concentrated (>1 M) NaOH solutions, several oxidation steps were thought to be involved, forming various products, including soluble indium species, an indium hydroxide layer, a porous hydrated film, and indium oxide. Other reports predicted different products from the anodic oxidation of indium [26–28]. The purpose of this paper is to gain a clearer understanding of the mechanisms involved in the anodic oxidation of indium in concentrated alkaline solutions.

2 Experimental

All electrochemical measurements were performed with a PGSTAT-30 (Autolab, Eco Echemie, Netherlands). The

H. Zhou · M. Xu
College of Materials Science and Engineering, South China University of Technology, 510641 Guangzhou, China

H. Zhou · M. Xu · Q. Huang · Z. Cai · W. Li
Key Lab of Electrochemical Technology on Energy Storage and Power Generation in Guangdong Universities, 510631 Guangzhou, China

Q. Huang · Z. Cai · W. Li (✉)
School of Chemistry and Environment, South China Normal University, 510006 Guangzhou, China
e-mail: liwsh@scnu.edu.cn

indium electrode was prepared from an indium rod with a purity of 99.99% (Alfa Aesar), and sealed with epoxy resin, providing an exposed area of 0.502 cm^2. Prior to taking measurements, the indium electrode was polished successively with silicon carbide waterproof paper (Westel grit: 800/P2400,) and 0.03 μm polishing powder (Westel), then degreased with acetone. A platinum foil and an Hg/HgO electrode in 3 M KOH were used as the counter and reference electrodes, respectively. All the potentials reported in this paper are with respect to the reference electrode. In the rotating ring-disc electrode (RRDE) measurements, a platinum ring and platinum disc, matched with an AFASR2E analytical rotator (Pine Instrument Company) were used. The indium disc electrode was obtained by electrodepositing indium onto the surface of a platinum disc at a potential of −1.4 V (relative to SCE) in a solution containing 0.025 M indium trichloride ($InCl_3$) plus 0.1 M potassium sulphate (K_2SO_4) at a pH of three for 5 min. The radius of the disc (r_1), insulating gap (r_2) and the ring (r_3) were 3.825, 3.985 and 4.215 mm, respectively. The theoretical collection efficiency (N) for the RRDE is 0.179.

The KOH solution was prepared with analytical-grade potassium hydroxide and double-distilled water. All measurements were performed at room temperature.

XRD was performed on a Rigaku D/MAX-RC (Japan) X-ray diffractometer equipped with a 30 kV, 30 mA X-ray tube, Cu target, and a 0.02° step size over the range $10° < 2\theta < 80°$.

3 Results and discussion

3.1 Voltammetric behavior with the rotating electrode

Voltammograms of the rotating indium disc platinum ring electrode in 3 M KOH solution with linear sweeping from an initial potential of −1.14 V to 0.7 V are provided in Fig. 1. The potential of the ring electrode was set at −1.3 V. An oxidation current peak is indicated at –0.94 V, with a wide shoulder between −0.75 V and 0.4 V. The indium experiences activation oxidation and passivation near the peak potential plus a secondary oxidation process within the wide shoulder potentials. Correspondingly, a larger reduction current can be recorded on the ring electrode, indicating that the anodic oxidation of indium is accompanied by the formation of soluble, reducible indium ions.

For the RRDE, the dependence on potential of the ratio of the ring current to disc current ($-i_r/i_d$) is illustrated in Fig. 2. The ratio remains essentially unchanged, at about 0.05, at the lower activation potentials, reaches a maximum of 0.160 (which is very close to the 0.179 theoretical collection coefficient for the RRDE) near the peak potential,

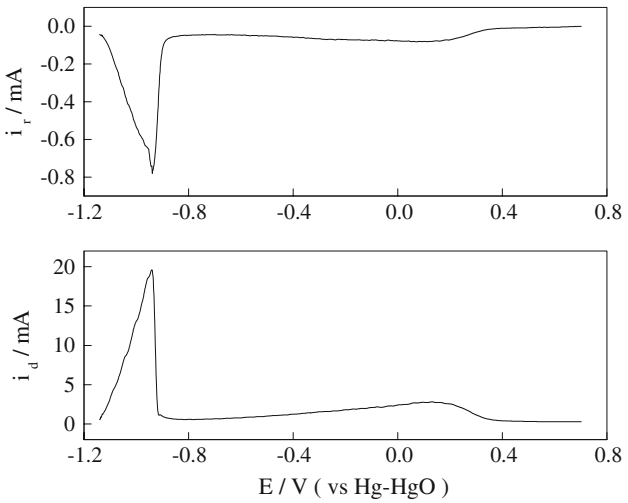

Fig. 1 Voltammograms of the rotating indium disc-platinum ring electrode in a 3 M KOH solution (the upper plot represents the ring, the lower the disk). The ring electrode potential was maintained at −1.3 V, with a 50 mV s^{-1} scan rate and rotational rate of 2,000 rev s^{-1}

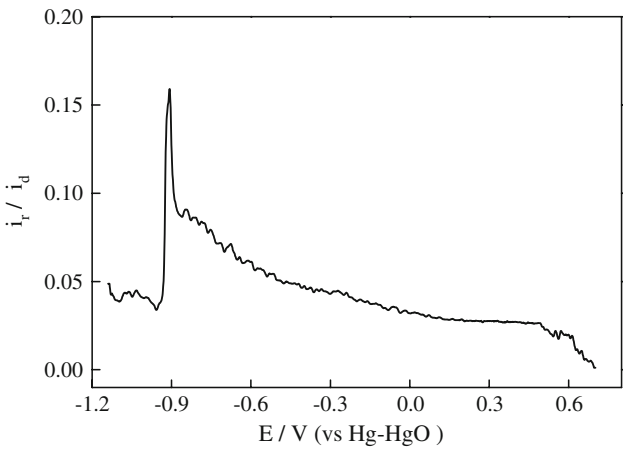

Fig. 2 Dependence of the ratio of ring current to disc current on potential for the RRDE

then decreases continuously to zero at potentials higher than the upper potential of the wide shoulder. This suggests that a portion of the products at the potentials in the activation and shoulder regions, and most of products at the peak potential are soluble, whereas the products formed above the upper shoulder region potential are insoluble.

3.2 Voltammetric behavior on a static electrode

The cyclic voltammogram of a static indium electrode in 3 M KOH solution, provided in Fig. 3, exhibits similar behavior to that of the rotating electrode during an anodic scan. There are some differences in the peak potential due to the physical differences between the electrodes.

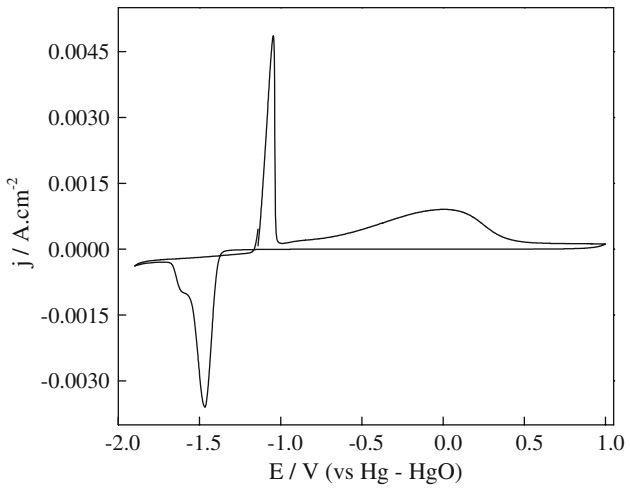

Fig. 3 Cyclic voltammogram of a static indium electrode in a 3 M KOH solution, at a 0.020 V s^{-1} scan rate

A reduction current peak at approximately −1.5 V and a slight shoulder can be observed during the cathodic scan.

To more clearly understand the reaction processes involved in the formation of the anodic oxidation peak, voltammograms at different potential scan rates were generated, and are presented in Fig. 4.

The oxidation peak current increases with scan rate, v. Generally, the total peak current can be represented as the sum of the charge-transfer and diffusion controlled currents [29]:

$$i_p = k_1 v + k_2 v^{0.5} \quad (1)$$

where k_1 and k_2 are constants. The first term, $k_1 v$, corresponds to the charge-transfer controlled current; the second one, $k_2 v^{0.5}$, to the diffusion-controlled current. The relationship between i_p/v and $v^{-0.5}$ is plotted in Fig. 5, which illustrates that i_p/v is linearly related to $v^{-0.5}$. The values of k_1 (3.7×10^{-6} A V^{-1} s) and k_2 (1.7×10^{-2} A $V^{-0.5}$ $s^{0.5}$)

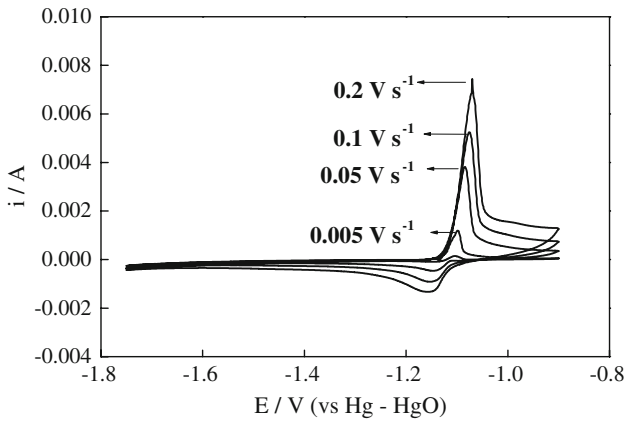

Fig. 4 Cyclic voltammograms of the static indium electrode in 3 M KOH at different scan rates. The initial, vertex, and final potentials are −1.14 V, −0.9 V, and −1.75 V, respectively

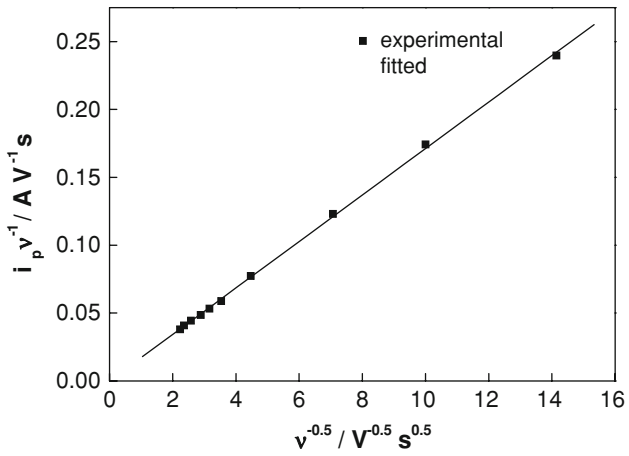

Fig. 5 Dependence of i_p/v on $v^{-0.5}$, using the data from Fig. 4

are obtained from the intercept and slope of the line. k_1 is much lower than k_2, which indicates that the reaction at the peak potential is basically diffusion-controlled.

3.3 Proposed mechanism for the anodic oxidation of indium

The relationship between peak potential (E_p, in mV) and scan rate for the diffusion-controlled reaction at 25 °C [25] satisfies:

$$d(E_p)/d(\log v) = 30/\alpha n \quad (2)$$

where the transfer coefficient α is equal to 0.5. Based on the slope obtained from Fig. 6, the electron number involved at the oxidation peak is 3, which is consistent with the result obtained by Saidman et al. [25]. Since the reaction product can be detected almost completely by the ring electrode, it can be inferred that the reaction at potentials close to the peak potential involves the formation of soluble In(III).

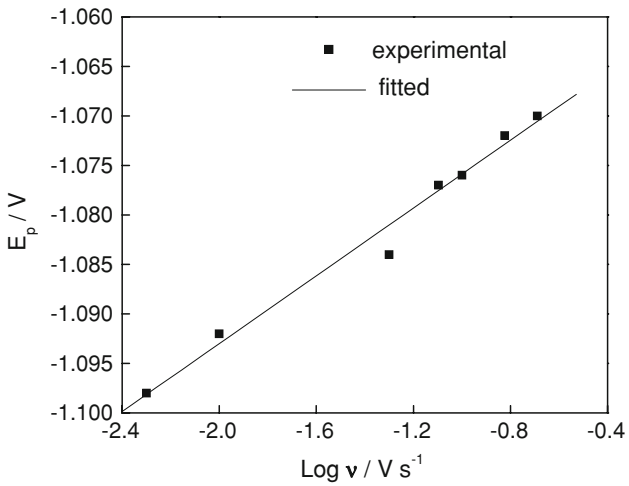

Fig. 6 Dependence of peak potential, E_p, on log v, using data from Fig. 4

Indium has two oxidation states: mono-valent In(I); and tri-valent In (III). Therefore, during the anodic oxidation of indium from the open circuit potential to the peak potential, it can be inferred that adsorptive, monovalent indium is formed:

$$In + OH^- \rightarrow In(OH)_{(ad)} + e^- \quad (3)$$

The monovalent indium is unstable and disproportionates to metallic indium and trivalent indium:

$$3In(OH)_{(ad)} + xOH^- \rightarrow 2In + In(OH)_{3+x}^{-x} \quad (x \geq 1) \quad (4)$$

The trivalent indium is soluble and can be detected by the ring electrode. This is why only a fraction of the anodic oxidation product can be detected in the activation region. At potentials approaching the peak potential, trivalent indium forms directly:

$$In + xOH^- \rightarrow In(OH)_x^{3-x} + 3e^- \quad (x \geq 4) \quad (5)$$

As the trivalent indium accumulating on the electrode surface reaches saturation, adhered :

$$In(OH)_x^{3-x} \rightarrow In(OH)_{3(ad)} + (x - 3)OH^- \quad (x \geq 4) \quad (6)$$

As soon as the adhered hydroxide covers the indium surface, further oxidation of indium is suppressed, resulting in the anodic oxidation peak on the voltammogram of indium. The presence of adhered hydroxide was confirmed by XRD. The XRD patterns of the indium electrode after polarization at −0.9 V (just at the foot of the peak on the positive side) for 10 min are presented in Fig. 7 along with the XRD pattern of pure $In(OH)_3$, illustrating that the polarized indium spectrum is characteristic of $In(OH)_3$ diffraction.

The adhered $In(OH)_3$, $In(OH)_{3(ad)}$, is unstable and can be dissolved through the reverse reaction of Eq. 6. This can be confirmed by the small oxidation peak (see Fig. 4) appearing during the cathodic scan at the potential near the peak potential during the anodic scan. The indium is exposed and oxidized as the adhered $In(OH)_{3(ad)}$ is dissolved. The oxidation peak was not observed by Saidman et al. perhaps because the NaOH concentration they used was too low for the deposited $In(OH)_3$ to be dissolved.

To understand the mechanism for the wide shoulder anodic oxidation of indium, cyclic voltammograms with different upper limit potentials were generated. The results indicate that the reduction peak current and potential are related to the applied upper limit potential, E_{ul}, as shown in Fig. 8. The more positive the upper potential applied, the more negative the reduction peak potential and the larger the reduction current.

The rate of increase of reduction peak potential, E_{rp}, is low for upper limit potentials below −0.9 V and above 0 V, but E_{rp} becomes more negative with increasing upper limit potential between −0.9 and 0 V, as illustrated in Fig. 9. This indicates that the products formed at potentials below −0.9 V and above 0 V are relatively well defined whereas those formed at potentials between −0.9 and 0 V are not.

The XRD pattern of the indium electrode, after having been polarized at 0.4 V for 10 min, compares closely with that of pure In_2O_3 powder, as illustrated in Fig. 10 (0.4 V is at the positive foot of the wide shoulder region). Whereas an XRD pattern does not provide definitive identification, it can be inferred that the product from the anodic oxidation of indium at higher potential is composed mainly of In_2O_3.

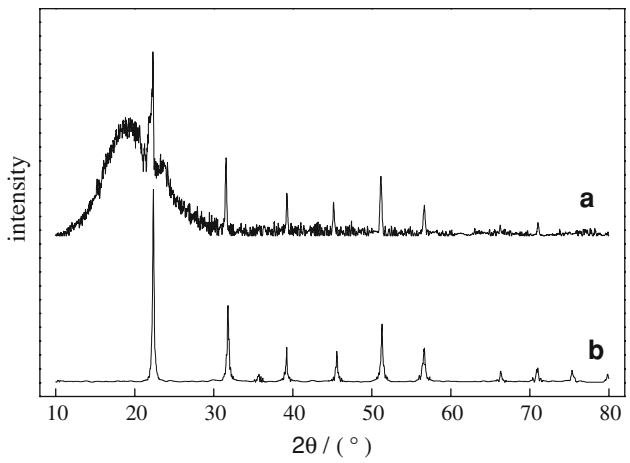

Fig. 7 XRD patterns of: (a) the indium electrode after polarization at −0.9 V for 10 min; (b) pure $In(OH)_3$ powder

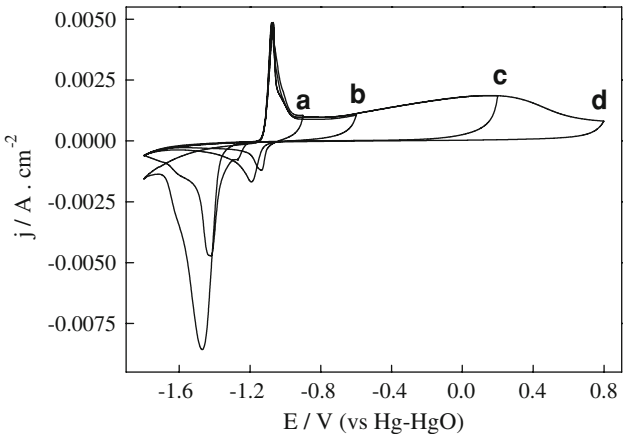

Fig. 8 Cyclic voltammograms for the static indium electrode in 3 M KOH solutions, at a scan rate of 0.020 V s^{-1}, with various upper limit potentials, (a) $E_{ul} = -0.9$ V, (b) $E_{ul} = -0.6$ V, (c) $E_{ul} = 0.2$ V, (d) $E_{ul} = 0.8$ V

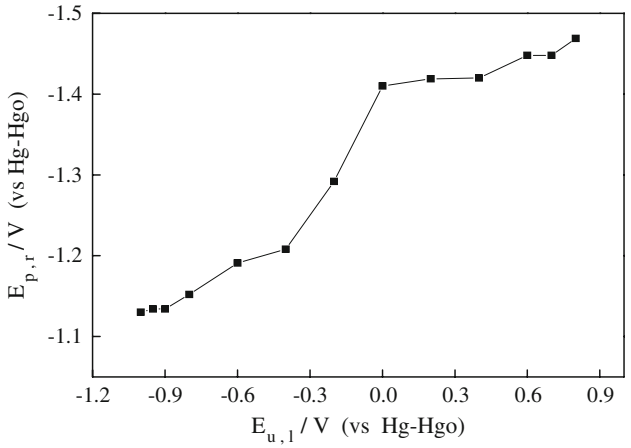

Fig. 9 Dependence of the reduction peak potential, E_{rp}, of anodic oxidation products on the upper limit potential, E_{ul}

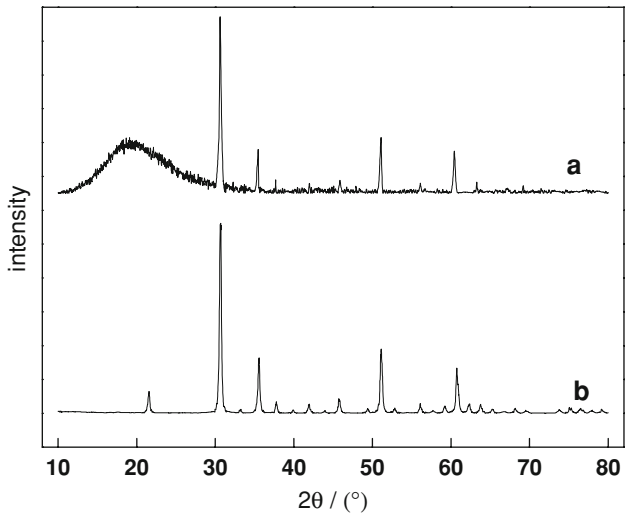

Fig. 10 XRD patterns of (a) the indium electrode after polarization at 0.4 V for 10 min and (b) pure In_2O_3 powder

The data generated indicate that the oxidation process at potentials greater than the anodic oxidation peak results in the dissolution of the adhered indium hydroxide:

$$In(OH)_{3(ad)} + (x-3)OH^- \rightarrow In(OH)_x^{3-x} \quad (x \geq 4) \qquad (7)$$

The newly-dissolved trivalent indium can be detected by the ring electrode. The indium underneath the adhered indium hydroxide is oxidized to In_2O_3:

$$2In + 6OH^- \rightarrow In_2O_3 + 3H_2O + 6e^- \qquad (8)$$

As the potential shifts positively, indium oxide accumulates between the adhered indium hydroxide and the indium matrix, resulting in the wide shoulder. In this region the anodic oxidation products of indium consist of $In(OH)_{3(ad)}$ and In_2O_3.

The In_2O_3 is more difficult to reduce than $In(OH)_{3(ad)}$ and hence more stable. This accounts for the dependence of the reduction peak potential on the upper limit potential, as indicated in Fig. 9. The reduction peaks at potentials lower than −0.9 V, between −0.9 V and 0 V, and above 0 V, correspond to the reduction of: $In(OH)_{3(ad)}$; the mixture of $In(OH)_{3(ad)}$ and In_2O_3; and In_2O_3, respectively. Their stability depends on the content of In_2O_3. The cathodic reduction for the higher upper limit potentials shows a shoulder after a reduction peak, as seen in Figs. 3 and 8. This may result from the reduction of other tri-valent indium species such as InO_2^-, which is formed from $In(OH)_x^{3-x}$ ($x \geq 4$), and is reduced with greater difficulty than In_2O_3.

4 Conclusions

Indium experiences two oxidation processes during its anodic polarization. In the first oxidation, soluble trivalent indium is the main product. This is formed from disproportionation of adsorbed monovalent indium hydroxide generated at lower potentials, and directly from the oxidation of indium at higher potentials. In the secondary oxidation, indium is oxidized directly to In_2O_3 under a layer of adhered $In(OH)_{3(ad)}$, which has been formed from saturated dissolved trivalent indium. In_2O_3 is more stable than $In(OH)_{3(ad)}$.

References

1. Metikos-Hukovic M, Omanovic S (1998) J Electroanal Chem 455:181
2. Li ST, Qiao XL, Chen JG et al (2006) Rare Met 25:359
3. Bandara J, Wansapura PT, Jayathilaka SP (2007) Electrochim Acta 52:4161
4. Araki N, Obata M, Ichimura A et al (2005) Electrochim Acta 51:677
5. Zhou HB, Yang MZ, Li WS (2008) Rare Metal Mat Eng 37:404
6. Zhou HB, Li WS (2005) J Chin Soc Corros Prot 25:25
7. Ren BY, Liu XP, Wang MH et al (2006) Rare Met 25:137
8. Schulte KH, Lewerenz HJ (1988) Electrochim Acta 43:1271
9. Morales AE, Zaldivar MH, Pal U (2006) Opt Mater 29:100
10. Stanimirova TJ, Atanasov PA, Stankova M et al (2007) Appl Surf Sci 253:8206
11. Yoshiyuki A, Tokuyuki N (2007) Mater Lett 61:3897
12. Bhuse VM, Hankare PP, Sonandkar S (2007) Mater Chem Phys 101:303
13. Ho WH, Yen SK (2006) Thin Solid Films 498:80
14. Lee CW, Sathiyanarayanan K, Seung WE et al (2006) J Power Sources 160:1436
15. Paramasivam M, Jayachandran M, Venkatakrishnaiyer S (2003) J Appl Electrochem 33:303
16. Zeinelabedin S, Saleh AO (2004) J Appl Electrochem 34:331
17. Perez M, O'Keefe MJ, O'Keefe T et al (2007) J Appl Electrochem 37:225

18. Watanabe CK, Nobe K (1976) J Appl Electrochem 6:159
19. Lovrecek B, Markovac V (1962) J Electrochem Soc 8:727
20. Muller B, Visco RE (1968) J Electrochem Soc 3:251
21. Omanovic S, Metikos-Hukovic M (1995) Thin solid films 266:31
22. Miyamoto K, Fukuju T, Sugimoto K (1997) Alkali secondary battery. Japan Patent: 5506076
23. Kordesch K, Weissenbacher M (1994) J Power Sources 52:217
24. Huang CA, Li KC, Tu GC et al (2003) Electrochim Acta 48:3599
25. Saidman SB, Bellocq EC, Bessone JB (1990) Electrochim Acta 35:329
26. Saidman SB, Bessone JB (1991) Electrochim Acta 36:2063
27. Duncan SJ, Burstein GT (1986) J Electrochem Soc 133:196
28. Salem TM, Ismail AA (1970) J Chem Soc (A) 2415
29. Bard AJ, Faulkner LR (1980) Electrochemical methods fundamentals and applications. Wiley, New York